The Astrophysical Journal, 678:L63–L66, 2008 May 1
© 2008. The American Astronomical Society. All rights reserved. Printed in U.S.A.

CORONAL γ-RAY BREMSSTRAHLUNG FROM SOLAR FLARE–ACCELERATED ELECTRONS

Säm Krucker,[1] G. J. Hurford,[1] A. L. MacKinnon,[2] A. Y. Shih,[1,3] and R. P. Lin[1,3]

Received 2008 February 12; accepted 2008 March 18; published 2008 April 3

ABSTRACT

The *Reuven Ramaty High Energy Spectroscopic Imager* (*RHESSI*) provides for the first time imaging spectroscopy of solar flares up to the γ-ray range. The three *RHESSI* flares with best counting statistics are analyzed in the 200–800 keV range revealing γ-ray emission produced by electron bremsstrahlung from footpoints of flare loops, but also from the corona. Footpoint emission dominates during the γ-ray peak, but as the γ-ray emission decreases the coronal source becomes more and more prominent. Furthermore, the coronal source shows a much harder spectrum (with power-law indices γ between 1.5 and 2) than the footpoints (with γ between 3 and 4). These observations suggest that flare-accelerated high-energy (∼MeV) electrons stay long enough in the corona to lose their energy by collisions producing γ-ray emission, while lower energetic electrons precipitate more rapidly to the footpoints.

Subject headings: Sun: flares — Sun: particle emission — Sun: X-rays, gamma rays

1. INTRODUCTION

The Sun accelerates electrons up to hundreds of MeV during solar flares (e.g., see review by Hudson et al. 2004). Collisions of these electrons with the ambient solar plasma produce X-ray and γ-ray emissions by the bremsstrahlung mechanism. X-ray and γ-ray observations therefore provide remote sensing diagnostics of flare-accelerated electrons. Since the frequency of collisions depends on the density of the ambient plasma, X-ray and γ-ray emission are most frequently observed from footpoints of flare loops as the density increases rapidly in the transition region. The density in the solar corona is generally too low to efficiently stop energetic electrons unless they are trapped there by other means. X-ray emissions from the corona are nevertheless observed, although generally fainter than the emissions from footpoints (Frost & Dennis 1971; Hudson 1978; Kane et al. 1992; Masuda et al. 1994; Veronig & Brown 2004; Battaglia & Benz 2006; Sui et al. 2006; Krucker et al. 2007a, 2007b). In flares occurring just behind the limb so that hard X-ray footpoints are occulted, faint coronal hard X-ray sources are observed in the majority of flares (Roy & Datlowe 1975; McKenzie 1975; Mariska et al. 1996; Tomczak 2001; Krucker & Lin 2008). Partially occulted observations of very large flares show coronal emissions up to the γ-ray range (Frost & Dennis 1971; Vestrand & Forrest 1993; Barat et al. 1994; Vilmer et al. 1999), but no imaging information was available at the time. This Letter presents observations in the X-ray and γ-ray range from the *Reuven Ramaty High Energy Solar Spectroscopic Imager* (*RHESSI*; Lin et al. 2002) that combine for the first time simultaneous imaging and spectroscopy.

2. OBSERVATIONS AND DATA ANALYSIS

RHESSI imaging (Hurford et al. 2002) uses nine bigrid rotating modulation collimators (RMCs). Behind each RMC is a cryogenically cooled germanium detector that provides high spectral resolution (∼1–10 keV FWHM) over the 3 keV–17 MeV energy range (Smith et al. 2002). As *RHESSI* rotates, the RMC transmissions vary rapidly, and imaging information is encoded in the resulting time modulation of the observed count rates. The *RHESSI* germanium detectors are electrically segmented into a front part and a rear part. The intense flux of low-energy X-rays (<200 keV) stops primarily in the front segment, allowing us to detect >200 keV γ-rays in the rear segment without significant dead time and pileup effects. Together with the *RHESSI* imaging capability, this provides for the first time imaging spectroscopy in the γ-ray range. The images taken above 200 keV presented in this Letter are all reconstructed from rear-segment data with the help of the CLEAN algorithm (Hurford et al. 2002) using subcollimators 4–9 (the grids in front of subcollimators 1–3 are not thick enough to efficiently modulate incoming counts above 300 keV). Subcollimators 4–9 generally show clear modulation, although subcollimator 4, which provides the finest spatial resolution (∼12″ FWHM), often provides only noisy images with a very limited dynamic range of ∼2. To reduce this noise in the subcollimator-averaged images, the same weighting for all subcollimators is used (i.e., natural weighting) in the images presented in this Letter, giving a spatial resolution of 23″ FWHM. At even higher energies (>500 keV), only two of the subcollimators (6 and 9) are thick enough to modulate the incoming γ-rays significantly and thus provide spatial information only at 37″ and 180″ FWHM scales.

The three *RHESSI* flares with the best counting statistics in the γ-ray range are presented in this Letter (Table 1). The rear-segment live time during the peak of these events was between 85% and 90% and even higher during the decay of the emission. The *RHESSI* coverage for the flare of 2005 January 20 was close to perfect, while for the other two flares only the later part of the event was seen by *RHESSI*. Therefore, the 2005 January 20 flare is first discussed in detail followed by brief summaries of the other two events.

2.1. *The 2005 January 20 Flare*

The *GOES* X7.1 class flare on 2005 January 20 occurred near the west limb (N14°W61°). The time profile in the 250–450 keV range (Fig. 1, *left*) is relatively simple with a major peak and an exponential decay that lasts roughly until the peak of the soft X-ray emission. The observed decay times are energy dependent and roughly scale with the square root of the energy (Fig. 1, *right*). Imaging in the 250–500 keV range during the peak of the emission shows the typical flare picture: electron bremsstrahlung emission originates from footpoints (Fig. 2, *left, blue contours*) of the flare loop that is seen in thermal X-rays below 20 keV (*red contours*). The dynamic range of the reconstructed *RHESSI* images of ∼10 gives an upper limit for the intensity of a coronal source hidden in the noise of ∼10% of the total flux. During the exponential decay, the 250–500 keV image shows, in additional to the footpoints, a third source cospatial (at least in projection) with the main flare

[1] Space Sciences Laboratory, University of California, Berkeley, CA 94720-7450; krucker@ssl.berkeley.edu.
[2] DACE/Department of Physics and Astronomy, University of Glasgow, Glasgow G12 8QQ, UK.
[3] Department of Physics, University of California, Berkeley, CA 94720-7300.

TABLE 1
SPECTRAL PARAMETERS AVERAGED OVER γ-RAY DECAY

Soft X-Ray Peak	*GOES*	Decay Interval (UT)	$\gamma_{\rm footpoint}$	$\gamma_{\rm corona}$
2003 Oct 28 11:10	>X17	11:12:05–11:19:54	3.8 ± 0.3	2.1 ± 0.4
2005 Jan 20 07:01	X7.1	06:46:38–06:53:18	2.9 ± 0.1	1.5 ± 0.2
2005 Sep 07 17:40	>X17	17:43:41–17:46:27	3.1 ± 0.1	1.6 ± 0.4

loop seen in thermal X-ray emission. As the decay progresses, the coronal source becomes more and more prominent, and it finally is the dominant emission late in the decay (Fig. 2, *middle*). At 250–450 keV, the decay time of the coronal source alone is ~550 s (Fig. 1, *bottom left*), while the footpoints decay faster (~200 s). *RHESSI* imaging at even higher energies (>500 keV) provides only a reduced spatial resolution of 37″, not enough to separate the coronal source from the footpoints in this event, so they are combined into a single elongated source (Fig. 2, *right*). The centroid position at 525–830 keV is closer to the coronal source than to the footpoints, suggesting that the coronal source is even brighter relative to the footpoints above ~500 keV. Imaging spectroscopy during the exponential decay (Fig. 3) indeed reveals that the coronal source has a harder spectrum ($\gamma = 1.5 \pm 0.2$) than the foopoints ($\gamma = 2.9 \pm 0.1$). Below 250 keV, emissions from the footpoints dominate and the limited dynamic range does not allow a clear identification of the coronal source. Around 450 keV, the coronal source and the combined footpoints are similar in intensity, while at higher energies the coronal source dominates. At energies above ~800 keV, counting statistics are too poor for imaging during the exponential decay except for the 2223 keV line emission. The 2215–2230 keV centroid position is located on the northern flare ribbon, not the coronal source (Fig. 2, *right*), indicating that during the decay, energetic protons (~10–100 MeV) are mostly losing their energy in footpoints of flare loops and not in the corona as is the majority of the >250 keV electrons. It is mentioned here that nuclear emission produced by flare-accelerated ions contributes only weakly to the γ-ray emission below 830 keV. Fits to the γ-ray spectrum show that about 15% of the emission in the 525–830 keV range is expected to be from nuclear processes for this flare (G. Share 2007, private communication). Assuming that all nuclear reactions are created at the footpoints as the 2223 keV emission makes the nonthermal bremsstrahlung component of the coronal source even more prominent than the 525–830 keV centroid position suggests (Fig. 2, *right*). Rough estimates show that the coronal source is about twice as bright as the combined bremsstrahlung emission in the two footpoints at 525–800 keV.

2.2. *The 2003 October 28 Flare*

The *GOES* >X17-class flare on 2003 October 28 occurred near disk center. *RHESSI* only started observing just before the soft X-ray peak time at 11:06 UT but nevertheless recorded the largest counting rates in the rear segments of all flares observed so far. The time profiles after 11:12 UT show an exponential decay similar to the 2005 January 20 flare with $\tau = (20 \pm 3)E^{0.54 \pm 0.08}$ lasting for more than 8 minutes, where E is the electron energy in keV. Flare-integrated *RHESSI* imaging results of this event are published by Hurford et al. (2006) showing that the 2.2 MeV emission produced by energetic protons comes from two sources, one on each of the flare ribbons, but displaced by ~15″ from the 200–300 keV footpoints. Next to the two electron bremsstrahlung footpoints, a fainter third source from in between the footpoints is also observed in the 200–300 keV image (Hurford et al. 2006, Fig. 2). The third source is at roughly (−80″, −390″) and seen only at the lowest contour level. Making an image during the exponential decay phase only (11:12:05–11:19:54 UT) clearly establishes the existence of this third source (Fig. 4, *left*). At this time, the third source is even the strongest source in the >250 keV range. Projection effects make it difficult to unambiguously place the third source in the corona, but the absence of EUV ribbons at the location of the in-between source makes a coronal explanation more likely. Although the error bars are large, the 2223 keV emission from this later time is located in between the flare ribbons and not from the third source (Fig. 4, *left*), indicating that energetic protons (~10–100 MeV) are still mostly losing their energy in footpoints. Imaging spectroscopy of the coronal source again reveals a very hard spectrum with $\gamma = 2.1 \pm 0.4$.

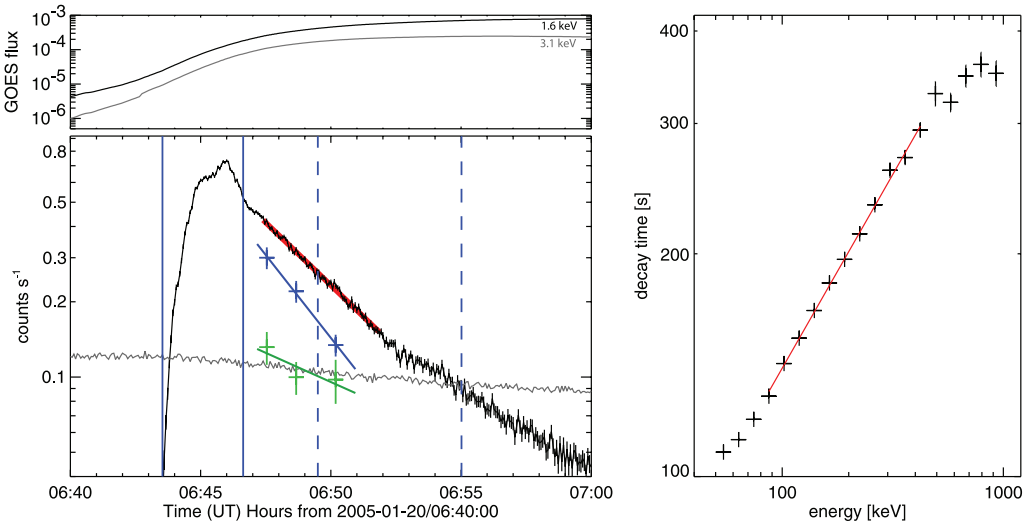

FIG. 1.—*Left:* Time profiles of the 2005 January 20 flare. *Top: GOES* light curves. *Bottom: RHESSI* rear-segment background-subtracted 250–450 keV time profile (*black*) and background (*gray*; determined from periods taken ±15 *RHESSI* orbits from the time of the flare). The green and blue curves give the separate time evolution of the coronal and footpoint sources. As these curves are derived by imaging spectroscopy, the time resolution is much coarser and the uncertainties are large. The vertical blue lines mark the time intervals of the two images shown in Fig. 2 (*left and middle*). The red line is an exponential fit to the 250–450 keV count rate with a decay time of 257 ± 2 s. *Right:* Energy dependence of the decay time. The red line is a power-law fit to the observations ($\tau \propto E^{0.52 \pm 0.08}$).

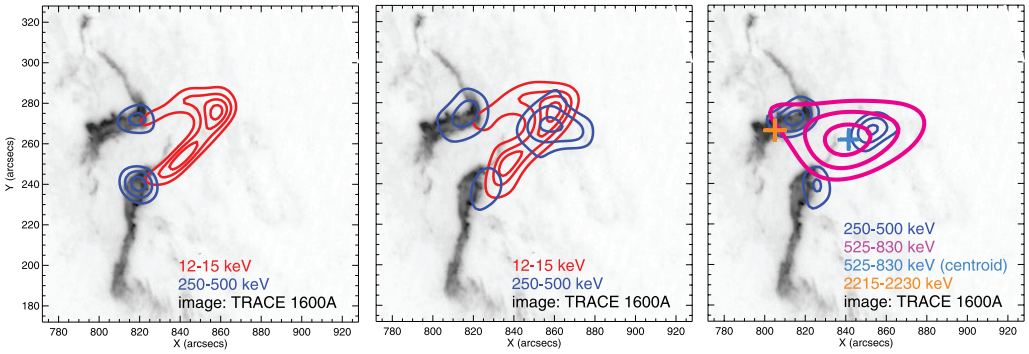

FIG. 2.—Imaging of the 2005 January 20 flare. *Left:* During the γ-ray peak (06:43:32–06:46:40 UT). *Middle:* During the end of the decay phase (06:49:30–06:55:01 UT). *Right:* Averaged over the decay phase (06:46:44–06:55:01 UT). All figures show a *TRACE* 1600 Å image taken at 06:45:11 UT. Thermal flare emission at 12–15 keV is shown in red contours, while nonthermal emission at 250–500 keV is given with blue contours. The 12–15 keV image is reconstructed using a MEM algorithm and the shown contour levels are 30%, 50%, 70%, 90%, while the CLEAN algorithm is used for the reconstruction of 250–500 keV images (23″ FWHM) and 50%, 70%, 90% contours are displayed. In the figure to the right, contours at 525–830 keV (*magenta*, levels are 50%, 70%, 90%) with a spatial resolution of 37″ FWHM are plotted, and the light blue and the orange crosses give the centroid position (center of mass) of the 525–830 keV and 2215–2230 keV emission with 1 σ error bars, respectively.

2.3. *The 2005 September 7 Flare*

The flare of 2005 September 7 occurred at the eastern limb. *RHESSI* only observed this flare during ~4 minutes just after the soft X-ray peak, but with high counting statistics. During this short time interval, the 250–500 keV flux is first exponentially decreasing ($\tau = 280 \pm 30$ s) then increasing again, possibly indicating a new injection. Imaging in the 200–400 keV range reveals footpoint emission at the limb and a second source above the limb (Fig. 4, *right*). This unambiguously shows the coronal nature of these emissions. Imaging spectroscopy again gives a very hard spectrum of the coronal sources with $\gamma = 1.6 \pm 0.4$.

3. DISCUSSION AND SUMMARY

The three *RHESSI* flares with best counting statistics above 200 keV show emission not only from chromospheric footpoints of flare loops but also from coronal sources. Since all of the three investigated flares show coronal emissions, coronal γ-ray sources could be a typical feature of a flare. To confirm this, a statistical study including all *RHESSI* γ-ray flares is in preparation. The coronal sources are most prominent during the decay of the γ-ray emission and have an extremely hard spectrum with a power-law slope between ~1.5 and ~2. The decay of the γ-ray flux shows surprisingly little deviation from a purely exponential decay, indicating a temporally stable interplay between electron acceleration, trapping, and energy losses. The parameters of the coronal sources are similar to the famous partly occulted flare recorded on 1969 March 30 (Frost & Dennis 1971) that showed coronal exponentially decaying emission ($\tau \sim 340$ s) with similar intensity and also a very hard spectrum ($\gamma \sim 2$), suggesting that the flares presented here are of the same kind. The observed spectral index of the coronal source in the 200–800 keV range is close to the theoretically hardest bremsstrahlung photon spectrum possible to observe (e.g., Brown et al. 2008), suggesting that the emission is produced by electrons at even higher energies (>1 MeV). Consequently, electrons at lower energies lose their energy by collision in footpoints. Similar behavior of high-energy electron trapping in solar flares is also reported from radio observations in the 10–100 GHz range (Melnikov & Magun 1998). Imaging of the 2223 keV line emission during the γ-ray decay phase for these flares suggests that ~10–100 MeV protons lose their energy in footpoints but not in the corona.

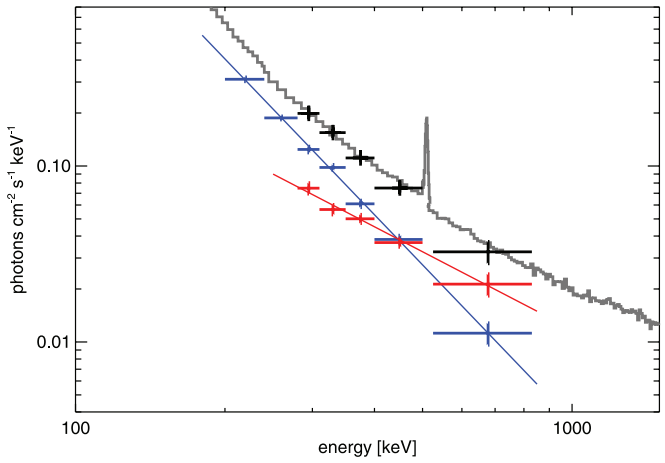

FIG. 3.—Imaging spectroscopy of the 2005 January 20 flare averaged between 06:46:44 and 06:55:01 UT. The spectrum of the coronal source and the combined footpoint sources are given in red and blue, respectively, and their sum is shown in black. The shown power-law fits give a much harder spectrum for the coronal source ($\gamma = 1.5 \pm 0.2$) than for the footpoints ($\gamma = 2.9 \pm 0.1$). For comparison, the higher resolution spatially integrated spectrum is shown in gray.

It is not the goal of this Letter to discuss detailed theoretical modeling of the presented observations, but only a short outlook on possible mechanisms is discussed in the following. As the collisional energy loss time, τ_c, of electrons with energies above 1 MeV is much longer than the transit time through the flare loop, trapping or confinement of electrons is needed to produce the observed coronal γ-ray emission. Since the magnetic field strength in the corona declines with increasing altitude, magnetic trapping can occur and a loss-cone electron distribution is formed. How long the loss-cone distribution lasts depends on how fast pitch-angle scattering is filling the loss cone. If the pitch-angle scattering time, τ_s, is shorter than the loss-cone formation time, the loss cone cannot be established. Otherwise, electrons scatter into the loss cone and precipitate to the footpoints of the loop (if $\tau_s < \tau_c$), or they are trapped until they lose all their energy by collisions ($\tau_s > \tau_c$).

One possible pitch-angle scattering mechanism is scattering between the flare-accelerated electrons and whistler waves produced by the electromagnetic loss-cone instability (e.g., Kennel & Petschek 1966). Wentzel (1976) argued that electrons at low energies grow whistler waves very efficiently and scatter electrons into the loss cone very quickly ($\tau_s < \tau_c$), while whistler waves produced by high-energy electrons are damped (see Wentzel 1976 for details). Thus, trapping of electrons is possible only for the highest energies. However, Melrose & Brown (1976) noted that whistler wave growth

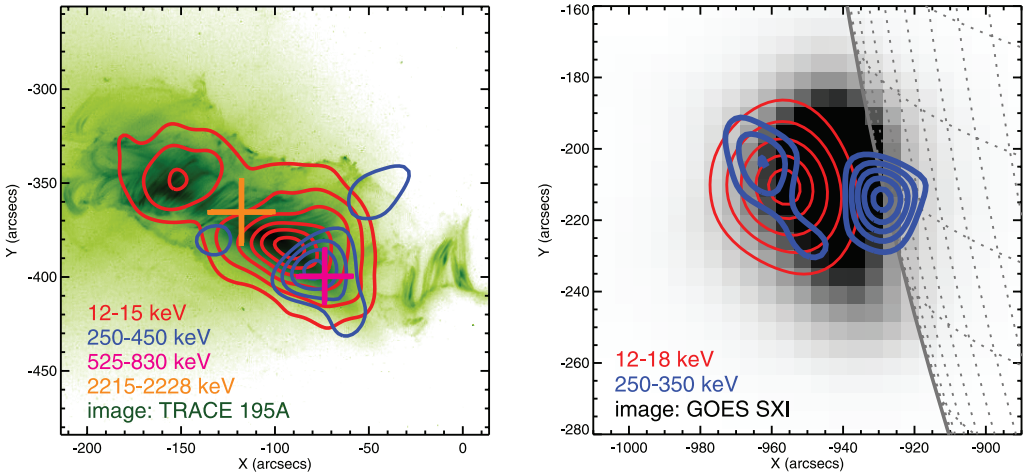

FIG. 4.—*Left:* Imaging of the 2003 October 28 flare. Contours of time-integrated (11:12–11:19 UT) CLEAN maps at 12–18 keV (spatial resolution is 17″ FWHM) and 250–450 keV (23″ FWHM) are plotted on a *TRACE* 195 Å image taken at 11:17:11 UT. The centroid positions of the 525–830 keV and 2215–2228 keV emission are plotted in magenta and orange, respectively. The shown contours levels are 7.5%, 15%, 30%, 50%, 70%, 90% and 50%, 65%, 80%, 95% for the 12–18 keV and the 250–450 keV emission, respectively. *Right:* Similar plot for the 2005 September 7 flare integrated during 17:43:41–17:46:27 UT. The shown image is taken by *GOES*/SXI at 17:43:06 UT. The contours levels are 35%, 50%, 65%, 80%, 95% for both energy ranges. The limb event of 2005 September 7 clearly shows the coronal nature of these emissions.

might not occur at low energies (<100 keV) as it is below the threshold energy. Before further conclusions on the importance of pitch-angle scattering by whistler waves can drawn, this topic has to be carefully revisited, which is not the focus of this Letter.

As collisions are always present, they always act as a pitch-angle scattering mechanism (e.g., Melrose & Brown 1976, MacKinnon 1991). At nonrelativistic energies, the pitch-angle scattering time and the energy loss time due to collisions are comparable (e.g., Petrosian 1985), and collisions can fill the loss cone before they lose all their energy in the corona. At relativistic energies, however, the scattering time scales with energy squared, while the energy loss time is proportional to energy, and electrons therefore lose their energy before they can fill the loss cone. This scenario describes the reported observations at least qualitatively as footpoints are dominant at low energies and a coronal source is seen at high energies. The decay time of the coronal source is then given by the energy loss time. At relativistic energies, synchrotron losses become important and the energy loss time of a trapped population is given by equation (7) in Petrosian (1985). With the observed value of $\tau_{\rm coronal} \sim 550$ s and $n = 4 \times 10^{10}$ cm^{-3} and an assumed coronal magnetic field of 50 G (200 G), the typical energy of the trapped electrons implied by the observed decay time in the January 20 flare becomes of the order of ~8 MeV (~10 MeV). This trapped population would produce an X-ray spectrum in the 200–800 keV range with a spectrum as hard as observed. If electron trapping in the corona is indeed stable for high-energy electrons, the corona would become a thick target (e.g., Brown 1971), and the total energy in energetic electrons above 8 MeV required to produce the observed coronal γ-ray emission in the 2005 January 20 flare would be of the order of 1×10^{28} ergs, or roughly $\sim 10^{-4}$ of a typical total energy of a giant solar flare.

If indeed collisions are the main pitch-angle scattering mechanism, a significant amount of coronal hard X-ray emission should also be produced at lower energies, in particular during the peak of the event. Theoretical calculations show (e.g., MacKinnon 1991, Fig. 6) that, depending on the ambient coronal plasma density and the loss-cone angle, coronal hard X-ray emissions below 100 keV can amount up to ~25% of the footpoint emission. Since the observed coronal emission during the peak is below the detection limit of 10%, the simple collisional pitch-angle scattering model can work only if the produced hard X-ray emission is below that limit. Furthermore, the energy dependence of the observed decay times should be matched. A detailed comparison of observations and model calculations is in preparation.

The work was supported through NASA contract NAS 5-98033 for *RHESSI*.

REFERENCES

Barat, C., et al. 1994, ApJ, 425, L109
Battaglia, M., & Benz, A. O. 2006, A&A, 456, 751
Brown, J. C., 1971, Sol. Phys., 18, 489
Brown, J. C., et al. 2008, preprint (arXiv:0802.0621)
Frost, K. J., & Dennis, B. R. 1971, ApJ, 165, 655
Hudson, H. S. 1978, ApJ, 224, 235
Hudson, H. S., et al. 2004, in Solar and Space Weather Radiophysics, ed. D. E. Gary & C. U. Keller (Dordrecht: Kluwer), 153
Hurford, G. J., et al. 2002, Sol. Phys., 210, 61
———. 2006, ApJ, 644, L93
Kane, S. R., et al. 1992, ApJ, 390, 687
Kennel, C. F., & Petschek, H. E. 1966, J. Geophys. Res., 71, 1
Krucker, S., Hannah, I. G., & Lin, R. P. 2007b, ApJ, 671, L193
Krucker, S., & Lin, R. P. 2008, ApJ, 673, 1181
Krucker, S., White, S. M., & Lin, R. P. 2007a, ApJ, 669, L49
Lin, R. P., et al. 2002, Sol. Phys., 210, 3
MacKinnon, A. L. 1991, A&A, 242, 256
Mariska, J. T., Sakao, T., & Bentley, R. D. 1996, ApJ, 459, 815
Masuda, S., et al. 1994, Nature, 371, 495
McKenzie, D. L. 1975, Sol. Phys., 40, 183
Melnikov, V. F., & Magun, A. 1998, Sol. Phys., 178, 153
Melrose, D. B., & Brown, J. C. 1976, MNRAS, 176, 15
Petrosian, V. 1985, ApJ, 299, 987
Roy, J.-R., & Datlowe, D. W. 1975, Sol. Phys., 40, 165
Smith, D. M., et al. 2002, Sol. Phys., 210, 33
Sui, L., Holman, G. D., & Dennis, B. R. 2006, ApJ, 645, L157
Tomczak, M. 2001, A&A, 366, 294
Veronig, A. M., & Brown, J. C. 2004, ApJ, 603, L117
Vestrand, W. T., & Forrest, D. J. 1993, ApJ, 409, L69
Vilmer, N., et al. 1999, A&A, 342, 575
Wentzel, D. G. 1976, ApJ, 208, 595